aerospace

MDPI

Article

Coupling Effect of Nonlinear Stiffness of Tape Spring Hinges and Flexible Deformation of Panels during Orbit Maneuvers

Wenyan Gu [1,2], Jinsheng Zhang [1,2], Longye Pan [1,2], Yegao Qu [3], Jin-Hwan Choi [4] and Xiangqian Zhu [1,2,*]

1 Key Laboratory of High-Efficiency and Clean Mechanical Manufacture, School of Mechanical Engineering, Shandong University, Jinan 250061, China; wygu@mail.sdu.edu.cn (W.G.); zhangjs@sdu.edu.cn (J.Z.); 201913924@mail.sdu.edu.cn (L.P.)
2 National Demonstration Center for Experimental Mechanical Engineering Education, Shandong University, Jinan 250061, China
3 School of Mechanical Engineering, Shanghai Jiao Tong University, Shanghai 200240, China; quyegao@sjtu.edu.cn
4 Department of Mechanical Engineering, Kyunghee University, Yongin 17104, Korea; jhchoi@khu.ac.kr
* Correspondence: xqzhu@sdu.edu.cn

Abstract: Many solar panels for spacecrafts are deployed by Tape Spring Hinges (TSHs) which have changeable stiffness. The stiffness of TSH is small when panels are folded, and it becomes large quickly in its deployed status. Since the solar panel is a thin sheet, flexible deformation is easily generated by orbit maneuvers. The coupling effect between the nonlinear TSHs and the flexible panels generates obvious vibration which affects the operational stability of the satellite. To investigate this coupling effect, non-deformable, linear deformable and nonlinear deformable panels were modelled by rigid body, modal order reduction method (MORM) and finite element method (FEM), respectively. The driving torque of TSH was described as a function of the rotation angle and angular velocity. The nonlinear properties of the TSH were reflected by one angle-stiffness spline multiplied by one stiffness coefficient. Dynamic responses of a satellite in deployment and orbit steering were analyzed by numerical simulations. Analysis results indicate the local deformation of panels keeps the stiffness of the TSH within a large range which accelerates the orbit maneuvers. However, much vibration is generated by the coupling effect if the luck-up status is broken up. The coupling effect affects the sequence of deployment, overshoot phenomenon and acceleration magnitude of the panels. Although the MORM is more efficient than FEM in computation, we propose FEM is better suited in the design of TSH and in studying the precise control of spacecraft with flexible solar panels and TSHs.

Keywords: flexible solar panel; tape spring hinge; nonlinear stiffness; coupling effect; orbit maneuver

Citation: Gu, W.; Zhang, J.; Pan, L.; Qu, Y.; Choi, J.-H.; Zhu, X. Coupling Effect of Nonlinear Stiffness of Tape Spring Hinges and Flexible Deformation of Panels during Orbit Maneuvers. *Aerospace* **2022**, *9*, 30. https://doi.org/10.3390/aerospace9010030

Academic Editor: Pierre Rochus

Received: 1 November 2021
Accepted: 29 December 2021
Published: 10 January 2022

1. Introduction

To achieve increased functionality and provide sustainable energy during space flight, ultra-light and ultra-thin solar panels are equipped to power the spacecrafts [1]. These thin panels have flexible deformation and vibrate during normal orbit maneuvers. Researchers have been seeking approaches that could analyze the on-orbit behavior of the spacecrafts equipped with thin solar panels. Solar panels are assumed to be rigid bodies or linear deformable bodies in most studies. Spacecraft and solar panels were modelled as rigid bodies by K.-W. Kim and Y. Park [2] in analyzing the deployment of solar panels. Honeycomb sandwich panels were modelled by Wang et al. [3] with respect to different equivalent modeling theories. The linear finite-element formulation and the linear modal approach with global mode shapes were used, respectively, by Wallrapp and Wiedemann [1,4] in modeling solar panels. The finite element modelling of the satellite sailboard was updated by Luo et al. [5] using sensitivity analysis. Nonmodal model reduction techniques were used to model flexible multibody systems by Fehr and Eberhard [6] with respect to the floating frame of reference framework. One three-axis stabilized spacecraft with

a pair of solar arrays was modeled as a discrete dynamic model by Liu et al. [7]. The accuracy of the modal approach depends on the quality of the mode shapes applied in the simulations [3]. However, neither the rigid body model nor modal order reduction method (MORM) model is adequate to express the nonlinear deformation of flexible bodies. Additionally, solar panels are frequently deployed by tape spring hinges (TSHs) which are typical self-deployable devices. TSHs are composed of one or several thin steel strips with a curved cross-section, and this curved cross-section provides small and large stiffnesses at the folded- and deployed statuses, respectively. Therefore, TSHs are used to deploy the folded panels slightly or to lock up the deployed panels firmly. The driving torque of the TSH has critical influence on the deployment of the panels. Both the numerical simulations and experiments tests were conducted to derive the expected driving torques in different statues. The two-ply plain-weave laminate of carbon-fiber reinforced plastic was used to make TSH by Mallikarachchi and Pellegrino [8], and the quasi-static driving torque of this TSH in folded and deployed statues were analyzed by using the commercial finite element package Abaqus/Explicit. The nonlinear dynamic behavior of thin-walled elastic structure was analyzed by Oberst and Tuttle [9,10] using experimental tests. The TSH made by a shape memory alloy dampened material was studied by Jeong et al. [11]. To attenuate the lock-up shock and overshoot motion, a new TSH made by Martensite detwinning of NiTi shape memory alloy was proposed by Lee et al. [12]. The self-locking phenomenon of TSH was studied specially by Hoffait et al. [13] using the finite element method. The bending behavior, quasi-static nonlinear behavior and nonlinear dynamics of TSHs were investigated by Dewalque et al. [14–16]. The steady-state moment and maximum stress of the TSH during deploying and folding processes were investigated using physics-based simulations by Ye et al. [17], and the geometry and structure of the TSH were selected by multi-objective optimization [18]. Large displacements and large rotations of folding TSHs were investigated by a planar rod model in Guinot et al. [19]. By means of the experimental measurements, Soykasap found the offset configuration yielded significant twisting moments [20]. Double-layer TSHs were designed by Yang et al. [21], and the section central angle, separated distance and the section radius of the TSHs were optimized to derive expected driving and locking torques. Except for the quasi-static behavior of the TSH, the influence of the joint clearance and coupling effect between the main-body of the satellite and panels are also research hotspots. The interaction effect between the TSHs and rigid solar panels during deployment was investigated by Kim and Park [2,22], and the expected TSH was validated through experimental tests by Kim et al. [23]. The coupling effect between the central rigid body and the solar arrays was analyzed by Wei et al. [24], and the global modes discretization technique was applied to investigate the elastic motion. The joint clearance between the rigid main-body and two flexible panels were investigated by Li et al. [25] by using nodal coordinate formulation and absolute nodal coordinate formulation, respectively. However, these investigations are merely about the characteristics of TSHs or the coupling effect between rigid solar panels and main-body, which are insufficient reflect the nonlinear deformation of panels.

Understanding the coupling effect of nonlinear stiffness of TSHs and nonlinear deformation of panels is important for TSH design and attitude control of satellite. H. Ren et al. [26] analyzed the dynamics and control strategies of a full-scale flexible electric solar wind sail spacecraft using both the reference nodal coordinate formulation and the floating frame of reference method. M. Borre and H. Flashner [27,28] presented a method for calculating all periodic solutions and their domains of attraction for flexible spacecraft model. Fonseca et al. [29] studied the effects of reaction wheels and piezoelectric transducers on the attitude and vibration control of a satellite with flexible solar arrays. Based on the semi-analytical solar radiation pressure model, Montenbruck et al. [30] studied the orbit-normal and yaw-steering attitude of QZS-1 spacecraft. The structural strain of the solar arrays was measured by Li et al. [31] in analyzing the vibration characteristics of solar arrays under deployment shock. Since the influence of the flexible appendages and the nonlinear TSHs on the stability of spacecrafts is unclear, it is of paramount importance to

analyze the coupling effect of the nonlinear deformation of panels and nonlinear stiffness of TSHs. Therefore, this coupling effect is figured out numerically for the cases of the deployment and orbit steering in this paper. To investigate the influence of the flexible deformation of panels, especially the nonlinear deformation, the solar panels were modeled by using three approaches which are rigid body, MORM and finite element method (FEM). Additionally, the TSH was modelled by revolute joint and driving torque which is function of the rotation angle and angular velocity. The nonlinear characteristics of the TSH was expressed by one angle-stiffness spline and one stiffness coefficient. The results given by the rigid body model imply merely the nonlinear TSHs are considered in the analysis. The coupling effect between the nonlinear TSH and the linear deformation of the panels is represented by the MORM model, while the coupling effect between the nonlinear TSHs and nonlinear deformation of the panels is considered by the FEM model. Since the rotation angles of TSHs and the accelerations of the panels indicate the deployment statue and vibration condition of the spacecraft, the influence of the coupling effect on the rotation angles of TSHs, accelerations and stress contours of panels were illustrated here. Analysis results indicate the coupling effect has non-negligible influences on the rotation angles of TSHs and acceleration magnitude of panels, which are not reflected by rigid body or by MORM. Although the MORM is more efficient than FEM in computation, the FEM is proposed in analyzing precise control of spacecraft with flexible solar panels and TSHs. This paper is organized as follows. The modeling of TSHs and solar panels are introduced In Section 2, and the panels are modeled by rigid body, MORM and FEM, respectively. In Section 3, two virtual maneuvers including deployment and orbit steering are designed to figure out the coupling effect. Finally, the main conclusions are drawn in Section 4.

2. Satellite System Model

Firstly, a satellite system composed of base, yoke and solar panels was modelled as rigid bodies, as shown in Figure 1. According to the LAPAN-constellation satellite [32], the mass properties of base, yoke and solar panels are listed in Table 1.

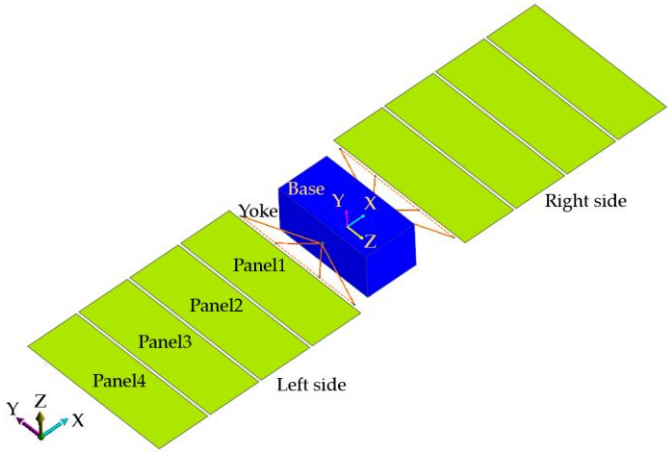

Figure 1. Model of a satellite system.

Table 1. Mass and moment of inertia of satellite system.

Items	Base	Yoke	Solar Panels
Mass (Kg)	1738.6	107.1	129.6
Jxx(kg·mm^2)	3.51×10^9	1.92×10^8	4.32×10^8
Jyy(kg·mm^2)	1.90×10^9	1.06×10^7	4.32×10^7
Jzz(kg·mm^2)	2.90×10^9	1.82×10^8	3.89×10^8
Jxy(kg·mm^2)	-8.27×10^7	-552.15	2.93×10^{-11}
Jyz(kg·mm^2)	-2.90×10^6	3.90×10^4	0
Jzx(kg·mm^2)	-8.27×10^7	85.86	9.76×10^{-12}

According to the structural of the LAPAN-constellation satellite, two TSHs were used to connect adjacent panels. Finally, there were nine TSHs for one side panels, as shown in Figure 2. Because the TSH has one rotational degree of freedom and provides driving torque, it was modeled by one revolute joint plus one driving torque herein. The driving torque, implemented by the rotational axial force of RecurDyn, is described as a function of the stiffness, damping, rotation angle, angular velocity and one angle-stiffness spline.

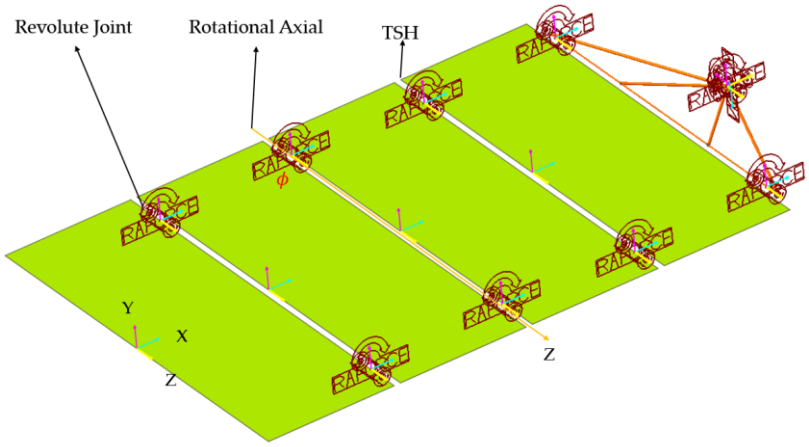

Figure 2. Modeling of tape spring hinges in RecurDyn.

2.1. Tape Spring Hinge

TSHs were composed of two elastic strips which were straight, thin-walled and had curved cross-section features, as showed in Figure 3. The folded TSHs coud be self-deployed by releasing stored strain energy. The mechanical properties of TSHs included high nonlinearity in the folding and deploying processes.

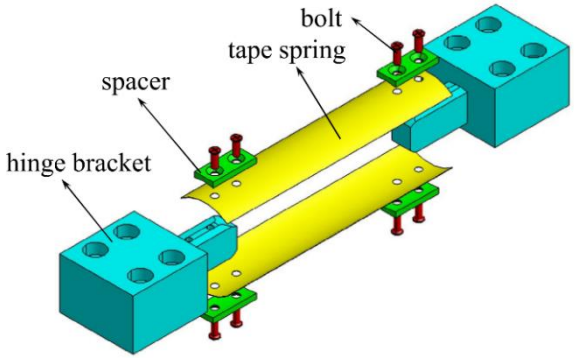

Figure 3. Tape spring hinge configuration [22].

The driving torque of a single TSH is described as the function of the stiffness, damping, rotation angle, angular velocity and one angle-stiffness spline in this paper. According to the experimental test, the stiffness of single tape strip can be implemented by the Akima spline function [33], which is a continuously differentiable interpolation built from piecewise third-order polynomials. Only data from the neighboring points are used to determine the coefficients of the polynomial. The driving torque of TSHs is described in Equation (1).

$$M = K \cdot \text{func}(\phi) - C \cdot \omega \quad (1)$$

where M is the driving torque; K and C are the stiffness and damping coefficient, respectively; ϕ, ω are the rotation angle and angular velocity between adjacent panels, respectively. The rotation axis is parallel with the Z-axis of satellite frame, and the rotation axis between the panels 2 and 3 is shown in Figure 2. The func(ϕ) represents nonlinear

stiffness spline which is a function of rotation angle ϕ, as shown in Equation (2). According to the user-subroutine function given in RecurDyn, the expression of the driving torque is shown here.

$$func(\phi) = \begin{cases} AKISPL(-((\phi 1 - \phi 2) + N{\cdot}90^\circ)) & \omega < 0 \\ -AKISPL((\phi 1 - \phi 2) + N{\cdot}90^\circ) & \omega = 0 \\ -AKISPL((\phi 1 - \phi 2) + N{\cdot}90^\circ) & \omega > 0 \end{cases} \quad (2)$$

where $\phi 1$ and $\phi 2$ are the rotation angles of two adjacent panels. AKISPL indicates the Akima spline function, and the spline interpolation is showed in Figure 4. According to the panels' initial positions and their expected position, N is -2, -1, 1 or 2. The stiffness in the unfolding process is small so that the panels are deployed gently, while the stiffness is enlarged sharply to lock the panels at deployment. The structural parameters of torsion spring are listed in Table 2. JYB means the driving torque between the Yoke and Base.

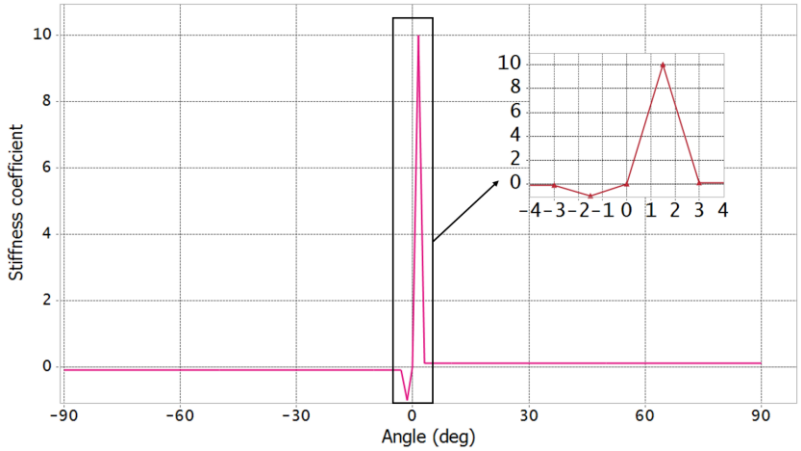

Figure 4. Nonlinear stiffness spline of single TSH.

Table 2. Structural parameters of torsion spring.

Torque Name	Stiffness(N/rad)	Damping(N·s/rad)
JYB (Yoke–Base)	350	75
J1Y (Panel 1–Yoke)	770	75
J21 (Panel 2–Panel 1)	955	75
J32 (Panel 3–Panel 2)	600	75
J43 (Panel 4–Panel 3)	440	75

2.2. Solar Panels

Solar panels are made of the ultra-light and ultra-thin materials, are extremely flexible and have low-frequency vibration modes [1]. These modes might resonate with motions of spacecraft in deployment and orbit steering. Therefore, it is essential to select proper approaches to model flexible solar panels and investigate their dynamic behaviors. The nonlinear deformation of the structure and local contact impact can be analyzed by FEM. MORM is suitable for analyzing the structures with linear deformation efficiently. To investigate the coupling effect between nonlinear TSHs and flexible panels, flexible solar panels were modelled by FEM and MORM, respectively.

2.2.1. Finite Element Method

FEM uses numbers of discrete elements to model the consistent body. All the element nodes assemble the stiffness matrix, putting in order the mass matrix and stiffness matrix of the structure. Every node has six degree of freedoms and can express the nonlinear deformation of the structure. In this section, RecurDyn software is used to carry out the finite element modeling of flexible solar panels. The solar panel was modelled as one

isotropy and uniform material, and the material properties of solar panels were defined according to the flexible substrate of the LAPAN-constellation satellite [32], which is shown in Table 3. The flexible array was modeled by the shell element Shell4 (quad4), and one flexible solar panel was modelled by 4145 nodes. The driving torque of the TSHs were transferred to two solar panels by multi-point constraint (MPC) [34] which includes 1 interface node and 34 slave nodes.

Table 3. Material properties of solar panel.

Parameters	Value
Length × width × thickness	6000 mm × 2000 mm × 4 mm
Density (ρ)	2700 kg/m^3
Modulus of elasticity (E)	70 GPa
Poisson's ratio (μ)	0.30

The flexible solar panel by FEM is shown in Figure 5.

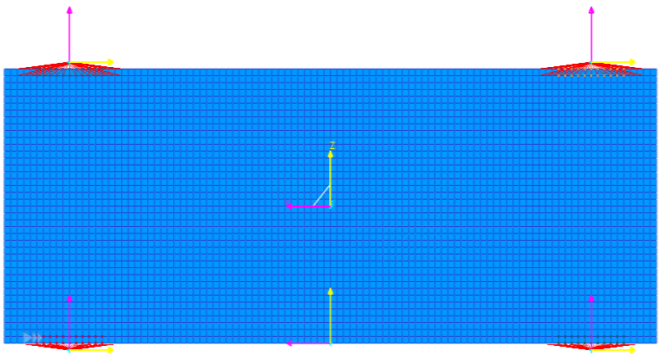

Figure 5. Flexible panel by FEM.

2.2.2. Modal Order Reduction Method

Multiple natural frequencies that appear easily system motion were selected as degrees of freedoms in MORM, and the structure linear deformations were expressed by the mode shapes of the selected frequencies. As the solar panels had already been modelled by FEM before, the mode shapes of panels could be easily calculated with respect to the principle of modal order reduction in RecurDyn. Except for the free modes, the constraint modes were also considered in this MORM model. One RFI file which contains all the information of selected frequencies and mode shapes was generated in this process. Since the joints and force items in MORM are the same with those in FEM, the flexible panels by MORM could be obtained easily by replacing the flexible panels with corresponding RFI files. The satellite with flexible panels is shown in Figure 6.

Some panels were constrained by two sides, while the outside panels were constrained by one side. The panels were named Panel 1, Panel 2, Panel 3 and Panel 4 from the main-body to the outside. Panel 1, Panel 2 and Panel 3 had four constraints points on two edges, and Panel 4 merely had two constraints points on one edge, as shown in Figure 6. The first 30 free modes and constraint modes were considered, and natural frequencies of the Panel 1 and Panel 4 are listed in Table 4. Some modes are shown in Figure 7.

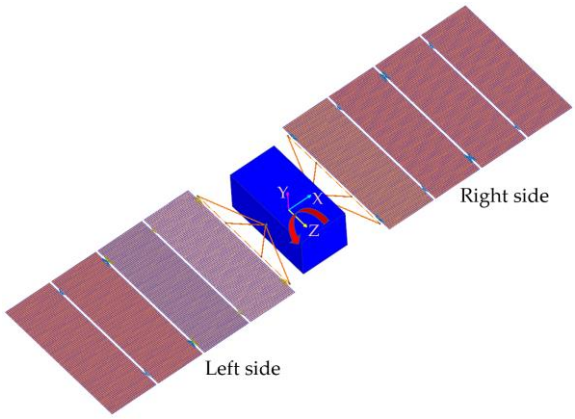

Figure 6. Satellite system with flexible panels.

Table 4. First 30 natural frequencies of Panel 1 and Panel 4.

Order \ Frequency (Hz)	Panel 1	Panel 4	Order \ Frequency (Hz)	Panel 1	Panel 4
1	0.59	0.59	16	12.16	11.59
2	1.10	1.09	17	13.20	11.78
3	1.67	1.65	18	15.05	14.10
4	2.42	2.33	19	15.09	15.01
5	3.44	3.32	20	15.45	15.33
6	3.92	3.80	21	16.60	15.49
7	5.46	5.45	22	16.80	15.74
8	5.76	5.54	23	16.91	16.71
9	5.81	5.60	24	19.19	17.20
10	6.12	6.00	25	19.35	18.80
11	7.37	7.22	26	20.29	19.67
12	8.38	8.03	27	22.15	20.49
13	9.37	8.51	28	22.58	21.14
14	9.57	9.20	29	24.77	21.97
15	12.07	11.31	30	25.06	26.50

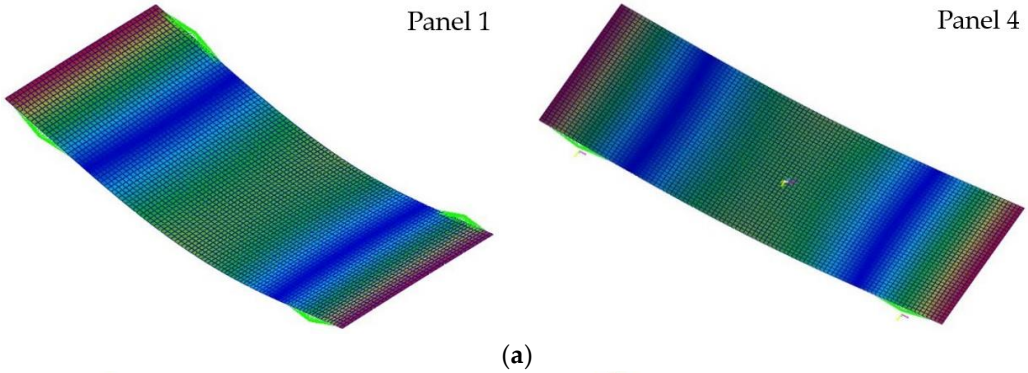

(**a**)

Figure 7. *Cont.*

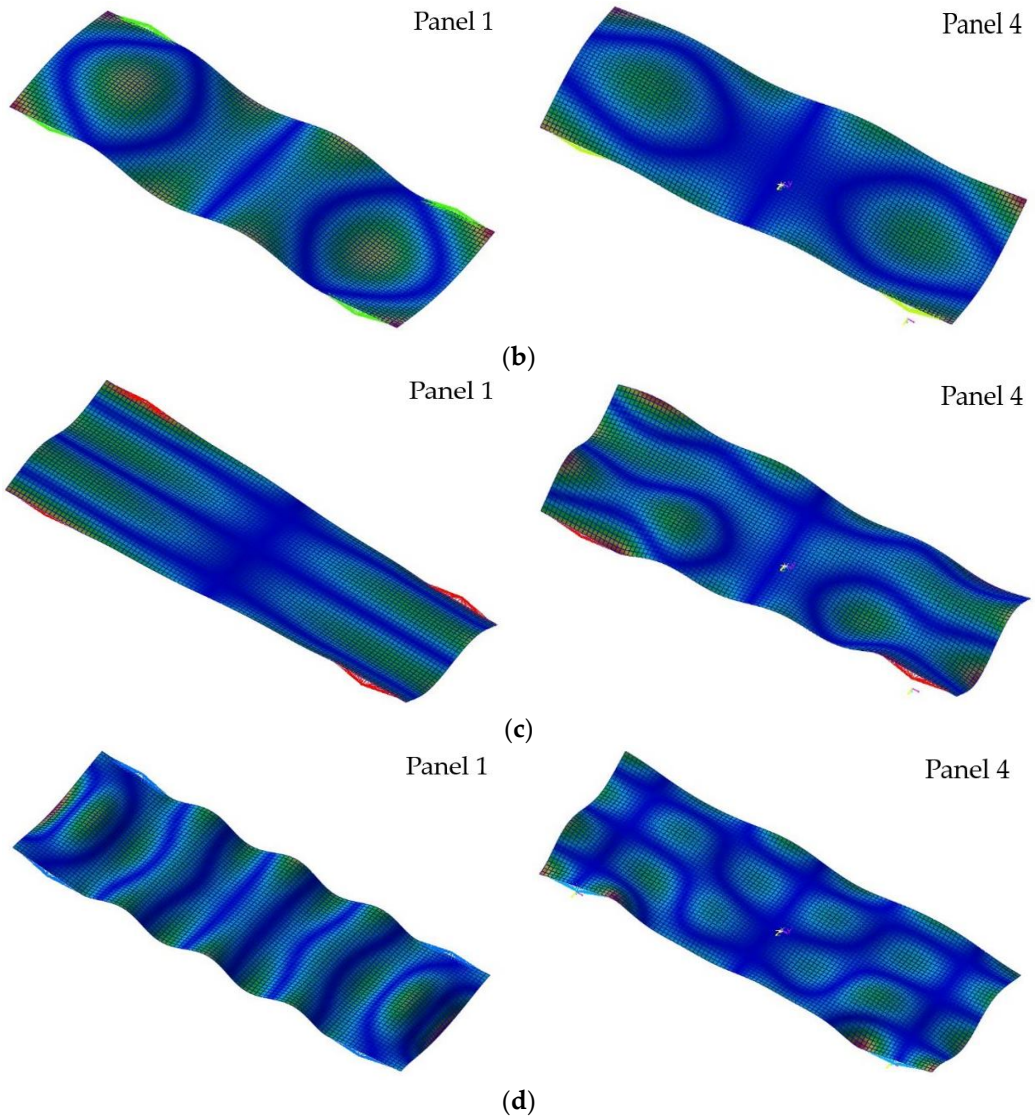

Figure 7. Modes of Panel 1 and Panel 4: (**a**) 1st mode; (**b**) 10th mode; (**c**) 20th mode; (**d**) 30th mode.

Because the number and distribution of constraints in Panel 1 were different to those in Panel 4, the vibration shapes of Panel 1 were also slightly different to those of Panel 4. For example, the frequency of the 30th mode of Panel 1 was 25.06 Hz, while it was 26.50 Hz in Panel 4. The modo shapes were also different as shown in Figure 7d.

3. Simulation Results

3.1. Deployment

The folded solar panels were stowed inside the launch vehicle fairing during the launch stage and were necessarily deployed in orbit using various deployment mechanisms [35]. The mission of satellites may fail if the deployment of solar panels is unsuccessful. Therefore, it was necessary to simulate the deployment of panels, and investigate whether panel vibration resonates with the deployment mechanisms. The deployment of flexible solar panels was simulated by using rigid body, FEM and MORM approaches, respectively. The rotation angles of TSHs, the maximum accelerations of panels and the stress contour of panels are illustrated herein.

All the panels were deployed successfully by each approach, as shown in Figure 8. This implies the stiffness and damping of the TSHs shown in Table 2 were selected properly. Although the satellite had slight asymmetry, as illustrated in Table 1, the right and left panels were deployed symmetrically by rigid model and MORM model. Meanwhile,

the panels far away from the base were deployed earlier than those closed to the base. The L_JYB and R_JYB were the last two TSHs to be deployed, and they met 0° at about 800 s. The Panel 4 and Panel 3 were the first and second panels to meet 0°, as shown in Figure 8a,b, respectively. Compared to the MORM model, the overshoot phenomenon was more obvious in the rigid model, as shown by R_J43/L_J43, and the rotation angles were regenerated from 0° at 170 s. Analysis results imply the linear deformation of panels relieved the inertia forces of panels. The stiffness of the TSH increased rapidly when the rotation angle was closed to 0°, and it bestowed the TSH with a self-locking function. The lock-up torque adhered the panel edges and generated local deformation. However, the local deformation was hard to express in the rigid body model or MORM model, while it was well expressed in the FEM model. Due to the coupling effect between the nonlinear deformation of panels and nonlinear stiffness of TSHs, the rotation angles of the left TSHs did not coincide with those of the right TSHs in the FEM model as shown in Figure 8c. The R_J21 and L_J43 were the first and second TSHs to meet 0°. Although the L_JYB and R_JYB were still the last two TSHs to be deployed, the R_JYB was about 90 s earlier than the L_JYB to meet 0°. The overshoot amplitude by FEM was larger than that by MORM, and the rotation angles of R_J43 and L_J32 were regenerated at 200 s. Additionally, much vibration was also generated in the rotation angle of TSHs.

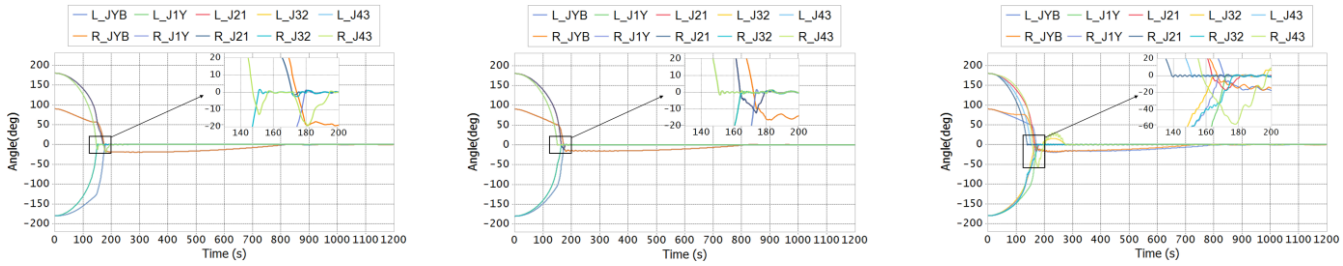

(**a**) (**b**) (**c**)

Figure 8. Rotation angles of TSHs in deployment: (**a**) by rigid body; (**b**) by MORM; (**c**) by FEM.

The acceleration of the middle point of panel edge was measured to investigate the vibration condition of panels. The acceleration of the rigid body model was much smaller than either the MORM model or the FEM model. Because the rotation angles of TSHs turned to 0° in Section A, the vibration condition of the MORM model was similar to that of the FEM model, as shown in Figure 9. Because the rotation angles of R_J43 and L_J32 were larger than 4° during 220~260 s in the FEM model, as shown in Figure 8c, the R_J43, L_J43 and L_J32 had slight effect on the vibration of Panel 1. As these TSHs affected Panel 1 in the MORM model, the vibration of the Panel 1 continued to 300 s. Because the R_J43 and L_J32 of FEM model turned to 0° at about 280 s, the lock-up torques regenerated accelerations in the Panel 1, as shown in the Section B of Figure 9. Section C illustrates the R_JYB and L_JYB of the FEM were deployed earlier than that of the MORM. The local deformation of panels consumed the kinetic energy of the panels, additionally, the local deformation also kept the TSH within a high stiffness range, so the panels of FEM came into a stabilization condition earlier than those of MORM model.

The stress contours of MORM model and FEM model at 280 s are shown in Figure 10. Generally, the Von Mises stress of the panels was less than 7.0 MPa which is much lower than the allowable stress. Because the R_J43 and L_J32 impacted with the stabilized panels in the FEM model, the local stress near the TSHs was larger by FEM than that by MORM. Although all the panels were deployed successfully here, the coupling effect between the nonlinear stiffness of TSHs and nonlinear deformation of panels affected the sequence of deployment and overshoot conditions. Therefore, the coupling effect should be considered in precise control of the attitude of the deployment and development of TSHs. Additionally, the MORM was much efficient than FEM, and the calculation times of deployment simulation by MORM and FEM were 192 min and 1672 min, respectively.

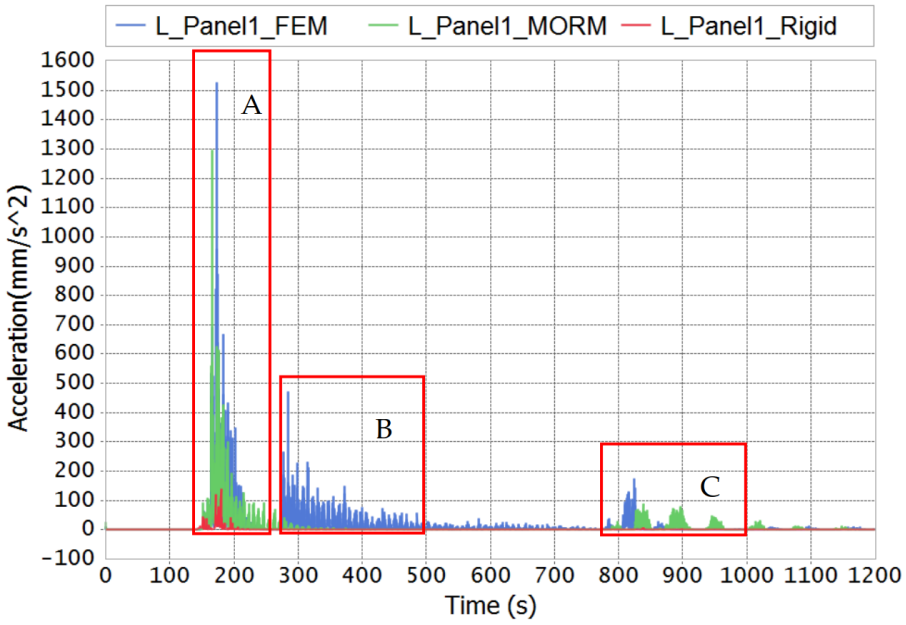

Figure 9. Accelerations of left Panel 1 in deployment by Rigid, MORM and FEM.

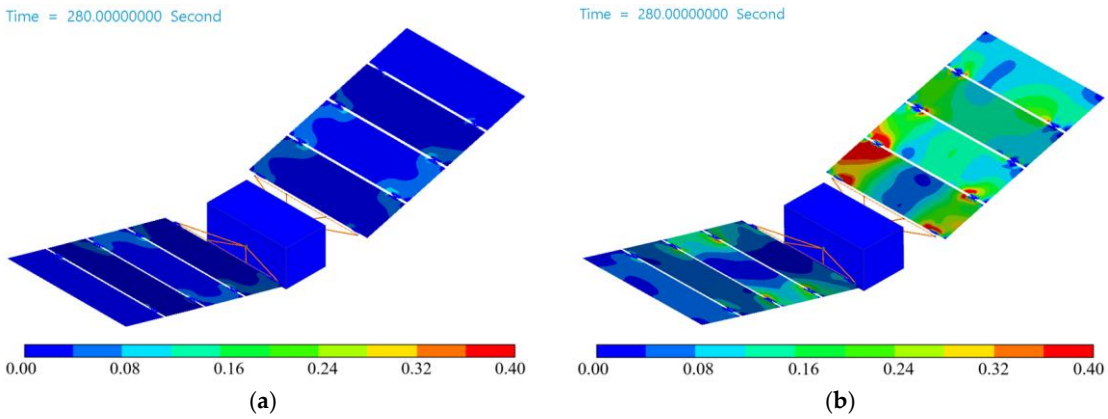

Figure 10. Stress contour of panels in deployment: (**a**) by FEM; (**b**) by MORM.

3.2. Orbit Steering

The orbit-attitude of the spacecraft was adjusted by gyroscopes sometimes, and this orbit steering generates panel vibration. Although the stiffness of the TSHs were large in deployed status, the deployed panels might rotate small angles around TSHs. The driving torques generated by these rotation angles might affect the orbit-attitude control system. Due to elastic deformation, the flexible panel exerted reaction forces on the main-body of the spacecraft and affected the orbit steering. Therefore, the steering motion of the spacecraft and the elastic deformation of the flexible panels were mutually coupled and affected. To investigate this coupling effect in orbit steering, the flexible solar panels were modelled by rigid body, MORM and FEM, respectively.

The control shaft momentum wheel provided torque to rotate the main-body of the satellite around one specified axis. The satellite enters the bias flight mode after reaching the preset angle. The satellite automatically returned to the normal attitude when the bias flight time was over. During steering, the bias flight mode control was consistent with the normal operation mode. The relation between the steering angle and time of the Michibiki, the first satellite of Japan's Quasi-Zenith satellite, as shown in Figure 11 [36]. According to the rotation speed of the Michibiki, the attitude angle of the satellite in orbit steering,

Ang was designed by Equation (3), where t is the simulation time. The base of satellite was rotated from right to left around the Z axis, as shown in Figure 6.

$$\text{Ang} = \begin{cases} 0^\circ & t < 10 \\ 30^\circ \cdot \left[\frac{t-10}{120}\right]^2 \left(3 - 2 \cdot \frac{t-10}{120}\right) & 10 \le t < 130 \\ 30^\circ & t \ge 130 \end{cases} \quad (3)$$

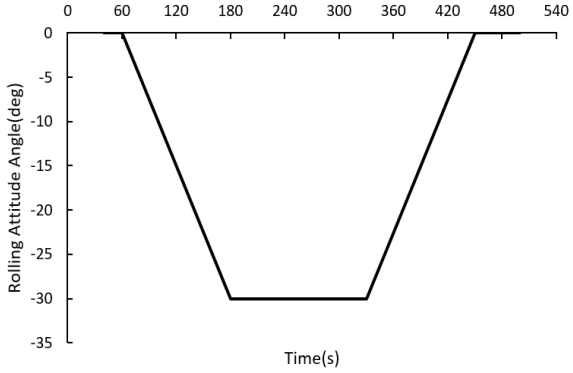

Figure 11. Time history of rotation angle in orbit steering [36].

The rotation angles of TSHs, panel accelerations and stress contour of panels are studied herein, and Figure 12 illustrates the rotation angles of the TSHs in orbit steering by rigid body, MORM and FEM, respectively.

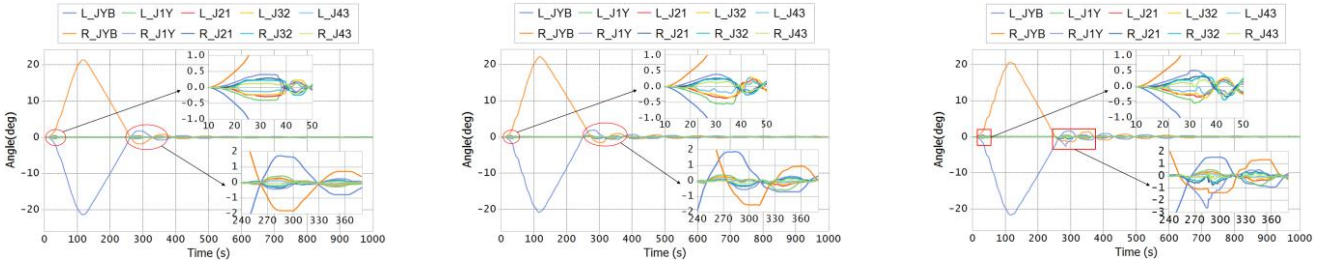

(**a**) (**b**) (**c**)

Figure 12. Rotation angles of TSHs in orbit maneuver: (**a**) by rigid body; (**b**) by MORM; (**c**) by FEM.

Generally, the satellite was steered successfully by every approach. Except for the R_JYB and L_JYB, all the other TSHs were locked well at the beginning of the steering since the maximum rotation angles of the TSHs were about 0.5°. According to the stiffness spline of TSH shown in Figure 4, the highest stiffness came about at 1.5°. The rotation angles of the R_JYB and L_JYB were slight larger than 20°, and there was not much difference in the rigid body model, MORM model and FEM model. Although the steering stopped at 130 s, it took about 230 s for the rotation angles of the R_JYB and L_JYB returning to 0°, as shown by the enlarged parts of the Figure 12a–c. The panels were rotated symmetrically in the rigid body model; the L_JYB returned to 0° earlier than the R_JYB in the MORM model; while the R_JYB returned to 0° earlier than the L_JYB in the FEM model. Therefore, the rotation angles were not symmetric in either the MORM or the FEM model. All the rotation angles were limited to the range of −2° to 2° in the MORM model. However, the rotation angle of R_J1Y exceeded 2° and had the tendency to break up the locking condition in the FEM model. Additionally, the rotation angles were changed smoothly in the MORM model, while much vibration was generated in the rotation angles of FEM model.

The accelerations of the middle point of panel edge are shown in Figure 13. As illustrated in Figure 12, the R_JYB and L_JYB were broken up at the beginning of the

steering and returned to 0° at about 250 s. Thus, the time history of the accelerations was divided into Sections D and E. The maximum acclamation of the rigid model was 6.9 mm/s^2, which was smaller than 10% of the values of the MORM and FEM models. The acceleration in Section E was larger than that in Section D, which illustrates much vibration was generated when the R_JYB and L_JYB were returned to 0°. The panels of the FEM model were returned to 0° earlier than those of the MORM model. Due to the coupling effect, the vibration of FEM model was much severer than that of the MORM model, and it was easily regenerated since two crests appeared in the acceleration of FEM model. This phenomenon cannot be reflected by MORM model which merely considers the coupling effect between the linear deformation of panels and the nonlinear stiffness of TSHs. The stress contours of MORM and FEM at 280 s are showed in Figure 14. The maximum Von Mises stress of the panels was less than 2.0 MPa. The local stress near the TSHs was larger in the FEM model than that in the MORM model, which is similar to the situation of deployment. The coupling effect between the nonlinear TSHs and nonlinear deformation of panels had a significant influence on the vibration condition of panels in the orbit steering. Due to the limitations of rigid body and MORM, the nonlinear deformation of panels could not be reflected, which might couple with the nonlinear driving torque of TSHs.

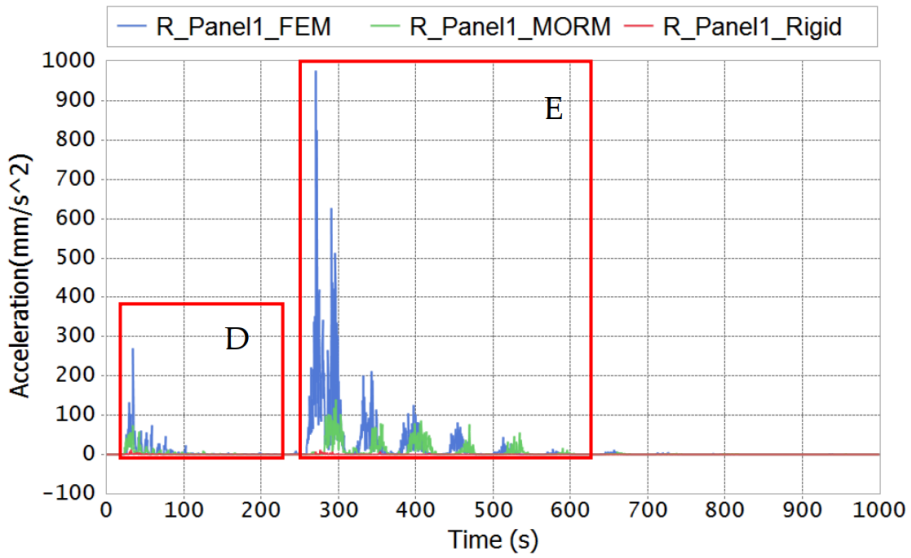

Figure 13. Accelerations of right Panel 1 in orbit steering by Rigid, MORM and FEM.

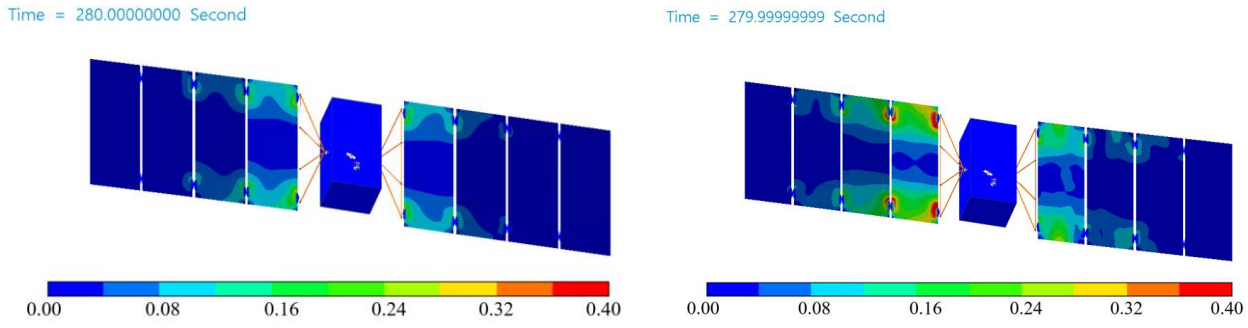

(**a**) (**b**)

Figure 14. Stress contour of panels in orbit maneuver: (**a**) by FEM; (**b**) by MORM.

4. Conclusions

The influence of the coupling effect between the nonlinear stiffness of TSHs and nonlinear deformation of panels on the deployment and orbit steering of the satellite

was analyzed by numerical simulation. The nonlinear TSH was modelled by a function of the stiffness, damping, rotation angle, angular velocity and one stiffness-angle spline. Additionally, the solar panels were modelled by rigid body, MORM and FEM, respectively. To illustrate this coupling effect, the rotation angles of TSHs and maximum acceleration of panels by rigid body and MORM were compared with those by FEM. The stress contours of panels were also shown to reflect the vibration condition. The analysis results are listed as follows:

(1) The linear deformation of panels relieves the inertia forces of panels and weakens the overshoot phenomenon in deployment. Meanwhile, the coupling effect enlarges the overshoot phenomenon.
(2) The left panels are deployed in coincide with the right panels by the rigid model and MORM model. The coupling effect affects the sequence of deployment, and the panels are deployed asymmetrically by the FEM model.
(3) The lock-up torque adheres the panel edges and generates local deformation in FEM model. The stiffness of TSH is kept in a large range by this local deformation. Panels are locked firmly if the local deformation and TSH can overcome the kinetic energy of the panels. Meanwhile, much vibration is generated if the local deformation and TSH cannot overcome the kinetic energy of the panels' rotation. Therefore, the stiffness of the TSH should be selected in considering of the local deformation of the panels and the kinetic energy of the panels. In other words, the speed of deployment and steering, the inertia properties of the spacecraft, the structure and material properties of the panels should be considered in design the stiffness of the TSHs.
(4) MORM is much more efficient than FEM in computation.

The self-deployable and self-locking functions of the TSH are sensitive to the rotation angle between two adjacent panels. The local deformation of panels should be considered to design expected TSH. Additionally, although MORM has better calculation efficiency, FEM should be used in studying the vibration of solar panels and precise attitude control of spacecraft with flexible solar panels and TSHs.

Author Contributions: Conceptualization, W.G., X.Z. and Y.Q.; methodology, W.G., J.-H.C. and X.Z.; software, J.-H.C.; validation, L.P. and W.G.; formal analysis, W.G.; investigation, W.G. and J.Z.; resources, J.Z. and Y.Q.; data curation, L.P. and W.G.; writing—original draft preparation, W.G.; writing—review and editing, X.Z. and J.-H.C.; visualization, L.P.; supervision, X.Z. and J.Z.; project administration, X.Z. and J.Z.; funding acquisition, Y.Q. All authors have read and agreed to the published version of the manuscript.

Funding: This work was supported by National Natural Science Foundation of China (Grant No.51909145); Key Laboratory of High-efficiency and Clean Mechanical Manufacture at Shandong University, Ministry of Education; National Demonstration Center for Experimental Mechanical Engineering Education at Shandong University; Young Scholars of Shandong University and Rizhao Intelligent Manufacturing Institute; and the Fundamental Research Funds of Shandong University.

Institutional Review Board Statement: Not applicable.

Informed Consent Statement: Not applicable.

Data Availability Statement: The data presented in this study are available on request from the corresponding author.

Acknowledgments: The authors would like to acknowledge FunctionBay Inc. for providing RecurDyn license.

Conflicts of Interest: The authors declare no conflict of interest. The funders had no role in the design of the study; in the collection, analyses, or interpretation of data; in the writing of the manuscript, or in the decision to publish the results.

References

1. Wallrapp, O.; Wiedemann, S. Comparison of results in flexible multibody dynamics using various approaches. *Nonlinear Dyn.* **2003**, *34*, 189–206. [CrossRef]
2. Kim, K.-W.; Park, Y. Systematic design of tape spring hinges for solar array by optimization method considering deployment performances. *Aerosp. Sci. Technol.* **2015**, *46*, 124–136. [CrossRef]
3. Wang, W.; Luo, H.; Fu, J.; Wang, H.; Yu, C.; Liu, G.; Wei, Q.; Wu, S. Comparative application analysis and test verification on equivalent modeling theories of honeycomb sandwich panels for satellite solar arrays. *Adv. Compos. Lett.* **2020**, *29*, 0963693520963127. [CrossRef]
4. Wallrapp, O.; Wiedemann, S. Simulation of Deployment of a Flexible Solar Array. *Multibody Syst. Dyn.* **2002**, *7*, 101–125. [CrossRef]
5. Luo, H.; Wang, W.; Fu, J.; Jiao, L. Finite element model updating of satellite sailboard based on sensitivity analysis. *Shock. Vib.* **2019**, *2019*, 4547632. [CrossRef]
6. Fehr, J.; Eberhard, P. Simulation process of flexible multibody systems with non-modal model order reduction techniques. *Multibody Syst. Dyn.* **2011**, *25*, 313–334. [CrossRef]
7. Liu, L.; Cao, D.; Wei, J.; Tan, X.; Yu, T. Rigid-flexible coupling dynamic modeling and vibration control for a three-axis stabilized spacecraft. *J. Vib. Acoust.* **2017**, *139*, 041006. [CrossRef]
8. Mallikarachchi, H.; Pellegrino, S. Quasi-static folding and deployment of ultrathin composite tape-spring hinges. *J. Spacecr. Rocket.* **2011**, *48*, 187–198. [CrossRef]
9. Oberst, S.; Tuttle, S. Nonlinear dynamics of thin-walled elastic structures for applications in space. *Mech. Syst. Signal Process.* **2018**, *110*, 469–484. [CrossRef]
10. Oberst, S.; Tuttle, S.; Griffin, D.; Lambert, A.; Boyce, R. Experimental validation of tape springs to be used as thin-walled space structures. *J. Sound Vib.* **2018**, *419*, 558–570. [CrossRef]
11. Jeong, J.W.; Yoo, Y.I.; Shin, D.K.; Lim, J.H.; Kim, K.W.; Lee, J.J. A novel tape spring hinge mechanism for quasi-static deployment of a satellite deployable using shape memory alloy. *Rev. Sci. Instrum.* **2014**, *85*, 025001. [CrossRef]
12. Lee, C.-H.; Jeong, J.-W.; Kim, Y.-J.; Lee, J.-J. Deployment shock attenuation of a solar array tape hinge by means of the Martensite detwinning of NiTi Shape Memory Alloy. *Rev. Sci. Instrum.* **2016**, *87*, 035104. [CrossRef] [PubMed]
13. Hoffait, S.; Brüls, O.; Granville, D.; Cugnon, F.; Kerschen, G. Dynamic analysis of the self-locking phenomenon in tape-spring hinges. *Acta Astronaut.* **2010**, *66*, 1125–1132. [CrossRef]
14. Dewalque, F.; Rochus, P.; Brüls, O. Importance of structural damping in the dynamic analysis of compliant deployable structures. *Acta Astronaut.* **2015**, *111*, 323–333. [CrossRef]
15. Dewalque, F.; Collette, J.-P.; Brüls, O. Mechanical behaviour of tape springs used in the deployment of reflectors around a solar panel. *Acta Astronaut.* **2016**, *123*, 271–282. [CrossRef]
16. Dewalque, F.; Schwartz, C.; Denoël, V.; Croisier, J.-L.; Forthomme, B.; Brüls, O. Experimental and numerical investigation of the nonlinear dynamics of compliant mechanisms for deployable structures. *Mech. Syst. Signal Process.* **2018**, *101*, 1–25. [CrossRef]
17. Ye, H.; Zhang, Y.; Yang, Q.; Xiao, Y.; Grandhi, R.V.; Fischer, C.C. Optimal design of a three tape-spring hinge deployable space structure using an experimentally validated physics-based model. *Struct. Multidiscip. Optim.* **2017**, *56*, 973–989. [CrossRef]
18. Ye, H.; Zhang, Y.; Yang, Q.; Zhang, B. Quasi-static analysis and multi-objective optimization for tape spring hinge. *Struct. Multidiscip. Optim.* **2019**, *60*, 2417–2430. [CrossRef]
19. Guinot, F.; Bourgeois, S.; Cochelin, B.; Blanchard, L. A planar rod model with flexible thin-walled cross-sections. Application to the folding of tape springs. *Int. J. Solids Struct.* **2012**, *49*, 73–86. [CrossRef]
20. Soykasap, O. Analysis of tape spring hinges. *Int. J. Mech. Sci.* **2007**, *49*, 853–860. [CrossRef]
21. Yang, H.; Liu, R.; Wang, Y.; Deng, Z.; Guo, H. Experiment and multiobjective optimization design of tape-spring hinges. *Struct. Multidiscip. Optim.* **2015**, *51*, 1373–1384. [CrossRef]
22. Kim, K.-W.; Park, Y. Solar array deployment analysis considering path-dependent behavior of a tape spring hinge. *J. Mech. Sci. Technol.* **2015**, *29*, 1921–1929. [CrossRef]
23. Kim, D.-Y.; Choi, H.-S.; Lim, J.H.; Kim, K.-W.; Jeong, J. Experimental and numerical investigation of solar panels deployment with tape spring hinges having nonlinear hysteresis with friction compensation. *Appl. Sci.* **2020**, *10*, 7902. [CrossRef]
24. Wei, J.; Cao, D.; Wang, L.; Huang, H.; Huang, W. Dynamic modeling and simulation for flexible spacecraft with flexible jointed solar panels. *Int. J. Mech. Sci.* **2017**, *130*, 558–570. [CrossRef]
25. Li, Y.; Wang, C.; Huang, W. Dynamics analysis of planar rigid-flexible coupling deployable solar array system with multiple revolute clearance joints. *Mech. Syst. Signal Processing* **2019**, *117*, 188–209. [CrossRef]
26. Ren, H.; Yuan, T.; Huo, M.; Zhao, C.; Zeng, S. Dynamics and control of a full-scale flexible electric solar wind sail spacecraft. *Aerosp. Sci. Technol.* **2021**, *11*, 107087. [CrossRef]
27. Borre, M.; Flashner, H. *Global Analysis of Periodic Solutions for Flexible Feedback Systems*; Springer: New York, NY, USA, 2012.
28. Borre, M.; Flashner, H. Periodic Solutions for Flexible Structures Under Relay Feedback Control With Time Delay. In Proceedings of the ASME 2012 5th Annual Dynamic Systems and Control Conference Joint with the JSME 2012 11th Motion and Vibration Conference, Fort Lauderdale, FL, USA, 17–19 October 2012.
29. da Fonseca, I.M.; Rade, D.A.; Goes, L.C.; de Paula Sales, T. Attitude and vibration control of a satellite containing flexible solar arrays by using reaction wheels, and piezoelectric transducers as sensors and actuators. *Acta Astronaut.* **2017**, *139*, 357–366. [CrossRef]

30. Montenbruck, O.; Steigenberger, P.; Darugna, F. Semi-analytical solar radiation pressure modeling for QZS-1 orbit-normal and yaw-steering attitude. *Adv. Space Res.* **2017**, *59*, 2088–2100. [CrossRef]
31. Li, D.; Liu, W.; Caizhi, F. Dynamic Characteristics of Satellite Solar Arrays under the Deployment Shock in Orbit. *Shock. Vib.* **2018**, *2018*, 6519748. [CrossRef]
32. Ramayanti, S.; Budiantoro, P. Design analysis of solar panel structure LAPAN-Constellation Satellite using finite element method. *IOP Conf. Ser. Mater. Sci. Eng.* **2021**, *1041*, 012020. [CrossRef]
33. Akima, H. A new method of interpolation and smooth curve fitting based on local procedures. *J. ACM (JACM)* **1970**, *17*, 589–602. [CrossRef]
34. Yoon, K.-H.; Heo, S.-P.; Song, K.-N.; Jung, Y.-H. Dynamic impact analysis of the grid structure using multi-point constraint (MPC) equation under the lateral impact load. *Comput. Struct.* **2004**, *82*, 2221–2228. [CrossRef]
35. Kim, D.-Y.; Lim, J.H.; Jang, T.-S.; Cha, W.H.; Lee, S.-J.; Oh, H.-U.; Kim, K.-W. Optimal design of stiffness of torsion spring hinge considering the deployment performance of large scale sar antenna. *J. Aerosp. Syst. Eng.* **2019**, *13*, 78–86.
36. Hauschild, A.; Steigenberger, P.; Rodríguez-Solano, C. Signal, orbit and attitude analysis of Japan s first QZSS satellite Michibiki. *GPS Solut.* **2011**, *16*, 127–133. [CrossRef]